



Geophysical Research Letters

Supporting Information for

Tropical Cyclone Wind Waves Under a Changing Climate

Christian M. Appendini¹, Pablo Ruiz-Salcines¹, Rodrigo Duran^{2,3}

¹Laboratorio de Ingeniería y Procesos Costeros, Instituto de Ingeniería, Universidad Nacional Autónoma de México, Puerto de abrigo s/n, Sisal, Yucatán 97356, México.

²National Energy Technology Laboratory, 1450 Queen Avenue SW, Albany, OR

³Theiss Research, La Jolla, CA, 92037, USA

Corresponding author: Christian M. Appendini (cappendinia@iingen.unam.mx)

Contents of this file

Introduction
Text S1 to S5
Figures S1 to S9
Tables S1 to S3
References

Introduction

The text and figures in this file complement the information presented in the manuscript by providing more information that we consider interesting to the readers. We provide additional background information, additional methodology details, and a description and discussion of the results for individual GCMs.

Text S1.

The main source of wave information for the API meteocean recommendations is the Gulf of Mexico Oceanographic Study (GOMOS) developed by Oceanweather, Inc. (API, 2007, 2014), which has been constantly updated to include more recent events and also early 20th century events as they become available from the Atlantic Hurricane Database Re-analysis Project (HDR) (https://www.aoml.noaa.gov/hrd/data_sub/re_anal.html). GOMOS is a wave hindcast based on the analysis of all sources of information available for tropical cyclones, to create proprietary wind fields to force a third-generation wave model and characterize tropical cyclones derived waves with events starting in 1900 (Oceanweather Inc., 2015). It is relevant to note that the wind fields used in GOMOS may only incorporate critical information since the 1960s, as aircraft measurements are available since the 1950s, satellite information since the mid-1960s, and Stepped Frequency Microwave Radiometer data since 1988. Also, the Hurricane Database (HURDAT) dataset (Landsea & Franklin, 2013) is more reliable since the mid-1960s with the advent of satellite information (Landsea C, 2007). As such, the GOMOS14 hindcast, covering events from 1900 through 2014, only incorporates measured data for the forcing wind fields since the 1960s, so that the data between 1900 and 1960 will not have the same accuracy as the latest data. Also, the wave hindcast cannot be validated for data before wave measurements started at oil rigs in the GoM, and particularly when the broader instrumentation programs started by the National Oceanic and Atmospheric Administration (NOAA) through the National Data Buoy Center (NDBC) in the 1970s.

Text S2.

The synthetic events provide information on date, time, position, radius of maximum winds, and maximum wind speeds, used as input to the Emanuel & Rotunno (2011) parametric wind model, which is defined in Eq. (1). The choice of parametric wind model follows Lin & Chavas (2012) and Ruiz-Salcines et al. (2019) where Lin & Chavas (2012) determined the Emanuel & Rotunno (2011) model as the most accurate when compared to H*Wind data (Powell et al., 1998) from Atlantic basin events between 1998-2009, and Ruiz-Salcines et al. (2019) found it as the most accurate model to represent the wind fields of TC for wave modeling.

$$V_r = \frac{2r(R_{mw}V_m + \frac{1}{2}fR_{mw}^2)}{R_{mw}^2 + r^2} - \frac{fr}{2} \quad \text{Eq. (1)}$$

where R_{mw} is the radius of maximum winds, V_m is the maximum wind speed, r is the radial distance from the eye of the hurricane to any given point surrounding it, f is the Coriolis parameter, and V_r is the wind speed of the hurricane at radius r . For the axisymmetric component of the TC wind field, we employed an empirical surface wind reduction factor of 0.85 and an inflow angle following (Bretschneider, 1972). Following Lin & Chavas (2012) the effect of the surface background winds was included by using a reduction factor of 0.55 for the storm translation velocity and a counter-clockwise rotation of 20° .

Text S3.

The wave model validation was attained by comparing modeling results with National Data Buoy Center (NDBC) buoys 42001, 42002, 42003, 42039, 42040, 42055, and 42056, located at deep waters in the GoM, with exception of 42056 which is located in the western Caribbean Sea. The validation considered the data when an event was located within 200 km from the buoy to the TC eye position. The historical events evaluated span 1975 through 2020. The storm parameters were obtained from the Tropical Cyclone Extended Best Track Dataset (Demuth et al., 2006). The error indexes are shown in Table S3 and were obtained comparing the model results to measurements through their inverse cumulative distributions or quantile function.

Text S4.

To generate the return period maps we created a vector for each grid element with the maximum SWH value obtained for each synthetic event simulated, as well as for the historical events. We then applied the peak over threshold method using the 98th percentile and adjusted the Generalized Pareto distribution to the data, obtaining the SWH for different return periods. For the selected return periods we generated the maps using the corresponding value at each grid element. To determine the return periods at the API (2014) areas, we selected the mesh elements corresponding to each area:

- Western GoM between 92° W and 98° W
- Central GoM between 84° W and 92° W
- Eastern GoM between 82° and 84° W.

We merged the vectors corresponding to each area and performed the same extreme value analysis described above for each mesh element. The procedure described above is a simplified version of the grid pooling methods from Heideman & Mitchell (2009), who present a procedure for grid pooling at a specific point location. Grid pooling is performed in API recommendations so that the randomness of the TC tracks is diffused by assessing the wave conditions as similar in a particular area, nevertheless, it is not clear in API (2014) how the grid pooling is performed for each area.

Text S5.

The significant wave height bias obtained for synthetic events derived from each GCM are presented in Figure S2 for the mean values and Figure S3 for the 99%-ile, while the significant wave height representing mean conditions and percentiles 90, 95, and 99 are shown in Figure S4 for the present climate and Figure S5 for a future climate. As the synthetic events are derived using the oceanic and atmospheric conditions in each GCM, it is expected that the resulting wave conditions will reflect such conditions. To interpret the wave results in the present climate we use the values reported by Camargo (2013) for Genesis Potential Index (GPI) in the GCMs and Sea Surface Temperature (SST) difference between the GCMs and the Reynolds SST, as well as the difference obtained for each GCMs between the present climate and RCP 8.5 scenario for GPI, Potential Intensity (PI) and Wind Shear (WS). Please note that the values presented by Camargo (2013) correspond to the same GCMs used to derived the synthetic events used in this study, except for MPI, where Camargo (2013) uses the MPI-ESM-LR GCMs and this study uses MPI-ESM-MR.

For the present climate, we found that the negative bias obtained in the west GoM and Caribbean from the events derived from HADGEM, IPSL, and MIROC is a result of an underestimation of SST in the tropical Atlantic, while the high positive bias in the GoM between Louisiana and Florida is a result of a higher GPI in that area, leading to a higher concentration of TC in this area. The wave conditions obtained from events derived from MPI show an opposite pattern, with a positive bias in the Caribbean and southern GoM and a negative bias in the northern GoM. While the SST shows a small negative bias in the main development region (MDR), the GPI is very high in the western Caribbean and southern GoM, leading to high wave heights in all of our study domain. The wave conditions derived from CCSM show a negative bias over all of the study domain which is not clearly explained looking at the GPI nor the SST differences. The wave bias obtained using the events derived from GFDL shows a smaller bias, with positive bias in the Caribbean and a slight positive bias near the western Mexican GoM coast. The GFDL SST difference is the smallest together with CCSM, while GFDL is closer to the ensemble mean. While each GCM results in a particular bias, we see from Figure 2 in the main manuscript that the bias is reduced in the model ensemble.

In a future climate, we found that the waves resulting from the events derived from GFDL and MPI are the highest, as a result of more intense wind events, probably related to the GCM higher GPI and PI and lower WS in a future climate for the GFDL. Nevertheless in the MPI, Camargo (2013) shows lower GPI in a future climate for the Caribbean and the southern GoM, as well as lower PI and higher WS in the Caribbean. While such values cannot explain the higher waves in all the study area, the values reported by Camargo (2013) correspond to MPI-ESM-LR, while the synthetic events in this study were derived from MPI-ESM-MR (see Table S1). HADGEM and IPSL do not show an increase of GPI compared to the present climate, although they show a higher PI in the GoM for a future climate, so that the derived synthetic events generate higher waves in the northern GoM, while the waves in the Caribbean are much smaller. The HADGEM derived events result in stronger waves in the northern GoM compared to those derived from IPSL, as the WS in HADGEM is much stronger in the Caribbean and lower in the GoM, inhibiting the

formation of events affecting the Caribbean and southern GoM and leading to stronger waves in the northern GoM. Waves resulting from MPI derived events show a similar pattern as GFDL resulting waves, although less intense, probably as result of a smaller PI compared to GFDL. The waves resulting from CCSM derived events show a similar pattern in the present and future climates, with only a mild increase in the wave intensity. Such results can be a result of barely no changes in GPI between present and future conditions, and a small increase in PI in the GoM for a future climate. When observing the GPI and PI for the model ensemble reported in Camargo (2013) we find an overall increase in GPI and PI in the Atlantic region, explaining the increase in wave height for a future climate in our study area.

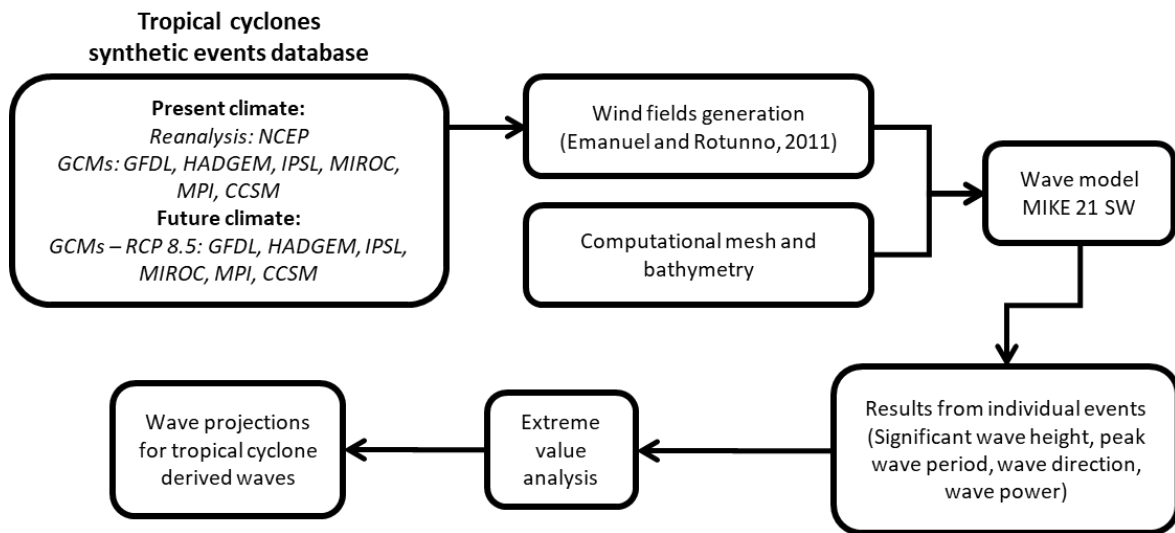


Figure S1. Flow diagram of the method employed in this study.

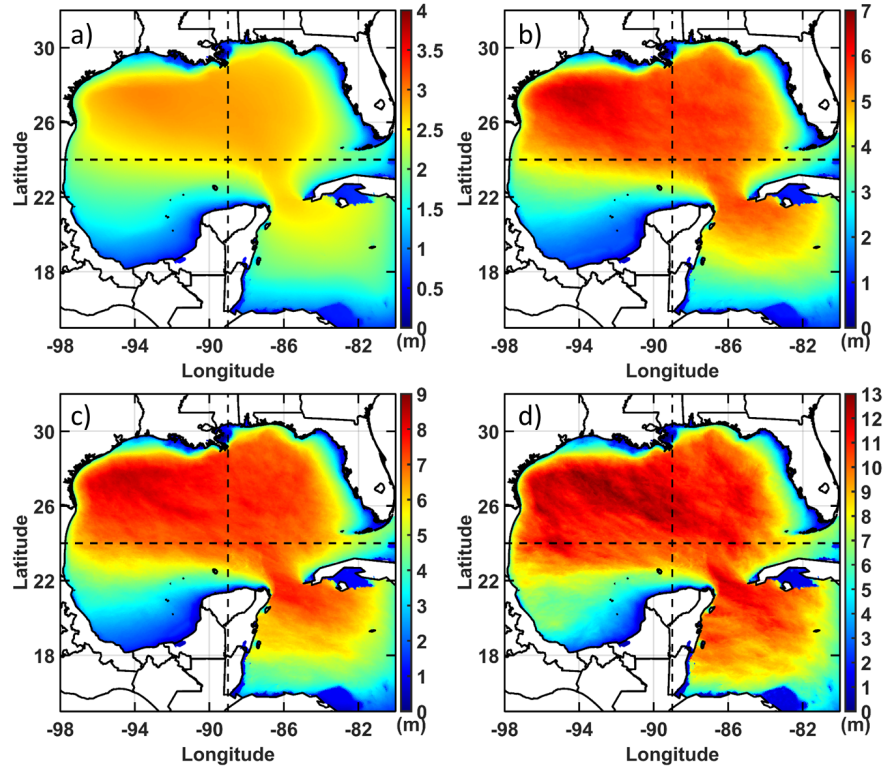


Figure S2. Significant wave height corresponding to percentiles a) 50, b) 90, c) 95, and d) 99, based on NCEP derived synthetic events.

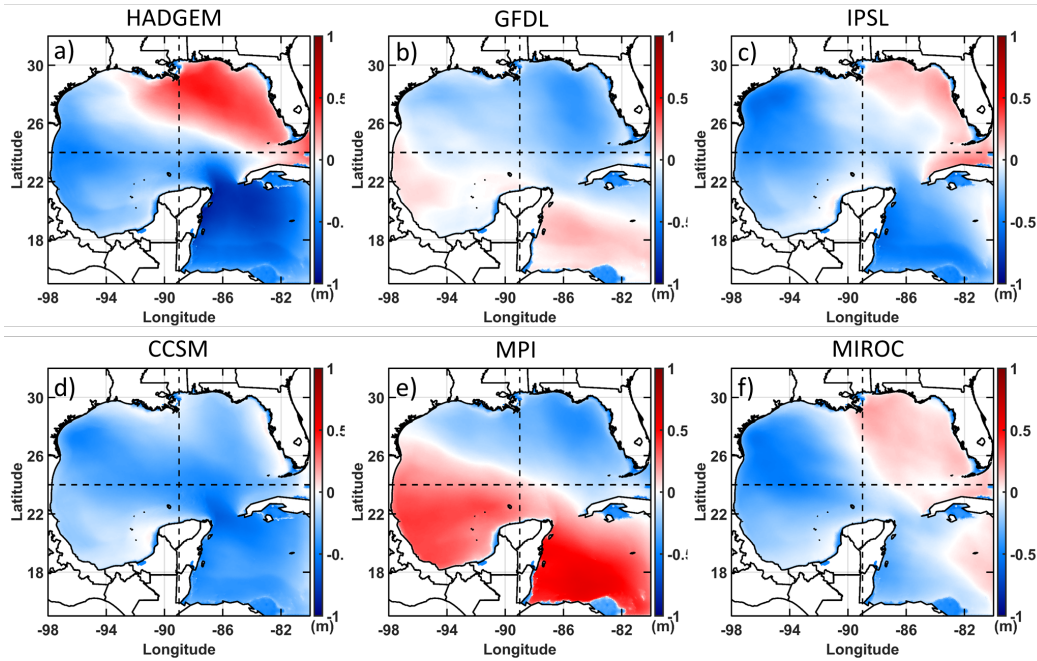


Figure S3. Global circulation model derived events present wave climate bias for significant wave height considering mean values. a) HADGEM, b) GFDL, c) IPSL, d) CCSM, e) MPI, f) MIROC.

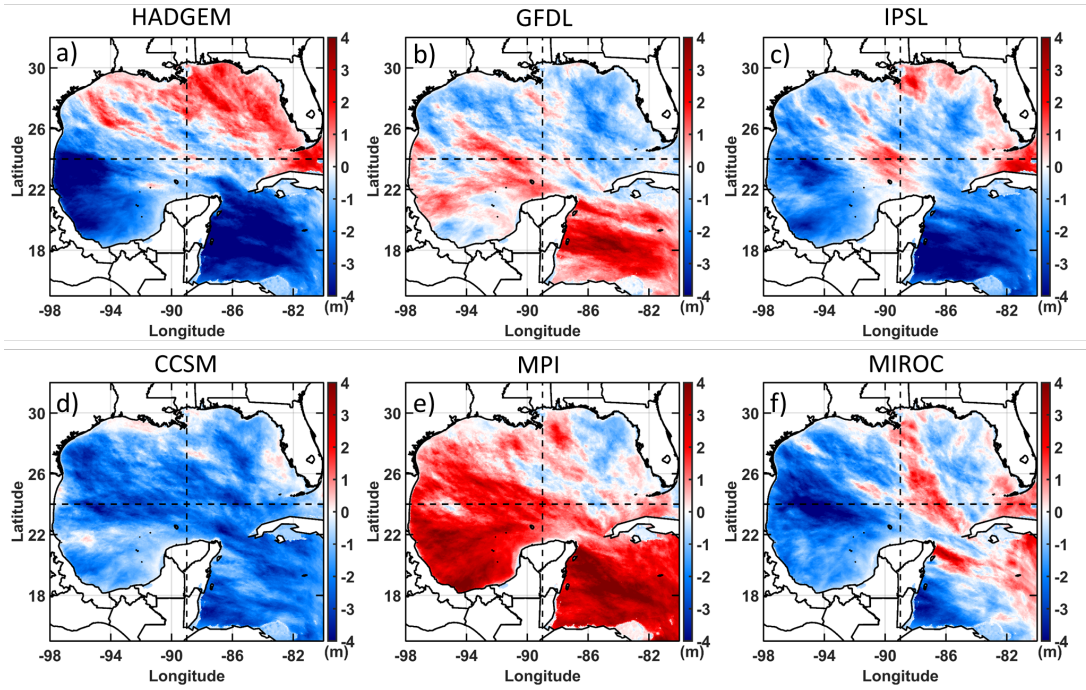


Figure S4. Global circulation model derived events present wave climate bias for significant wave height considering the 99%-ile values. a) HADGEM, b) GFDL, c) IPSL, d) CCSM, e) MPI, f) MIROC.

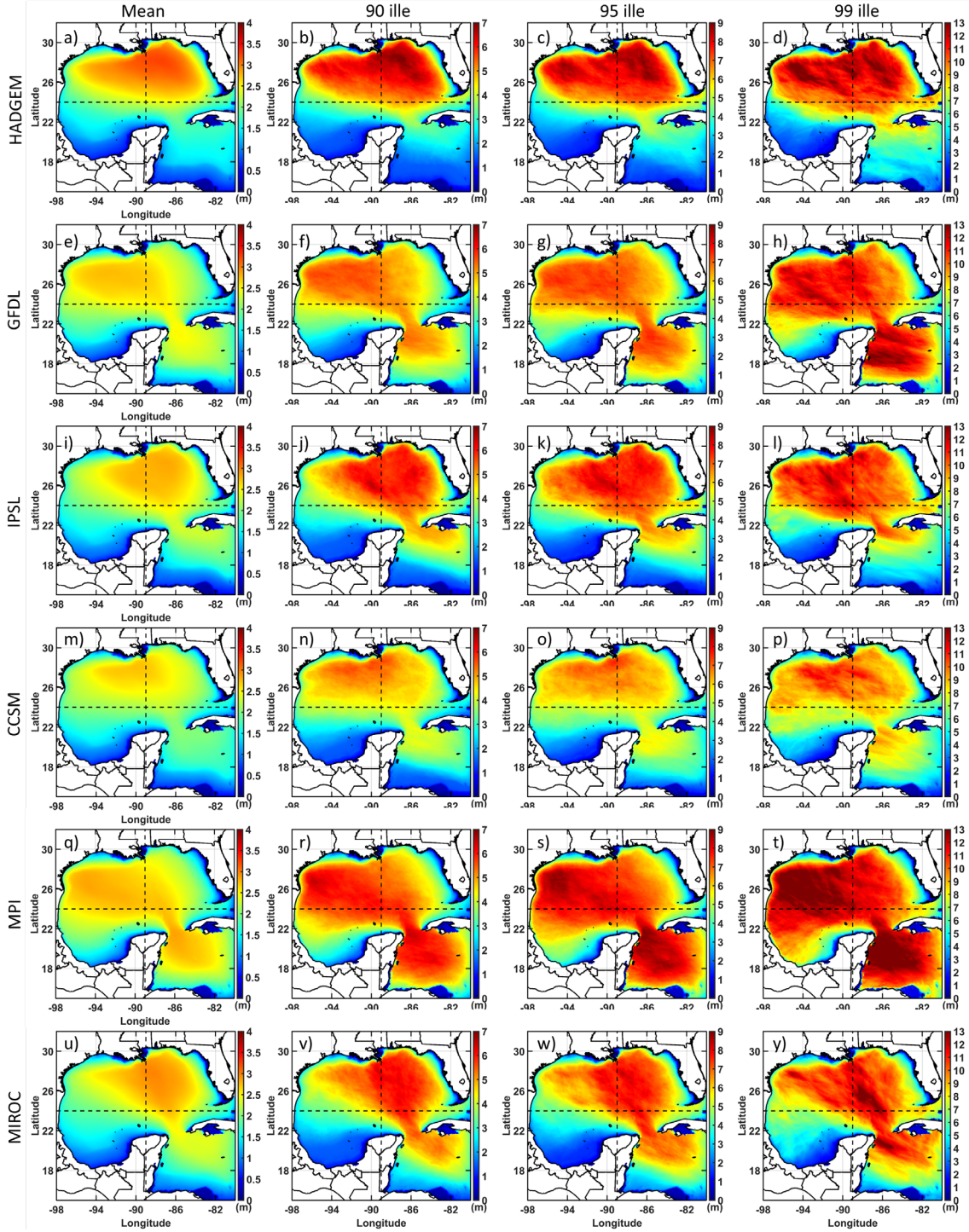


Figure S5. Global circulation models wave conditions for significant wave height in the present climate for HADGEM (a, b, c, d), GFDL (e, f, g, h), IPSL (i, j, k, l), CCSM (m, n, o, p), MPI (q, r, s, t) and MIROC (u, v, x, y) including mean (a, e, i, m, q, u), 90%-ile (b, f, j, n, r, v), 95%-ile (c, g, k, o, s, y) and 99%-ile (d, h, l, p, t, y).

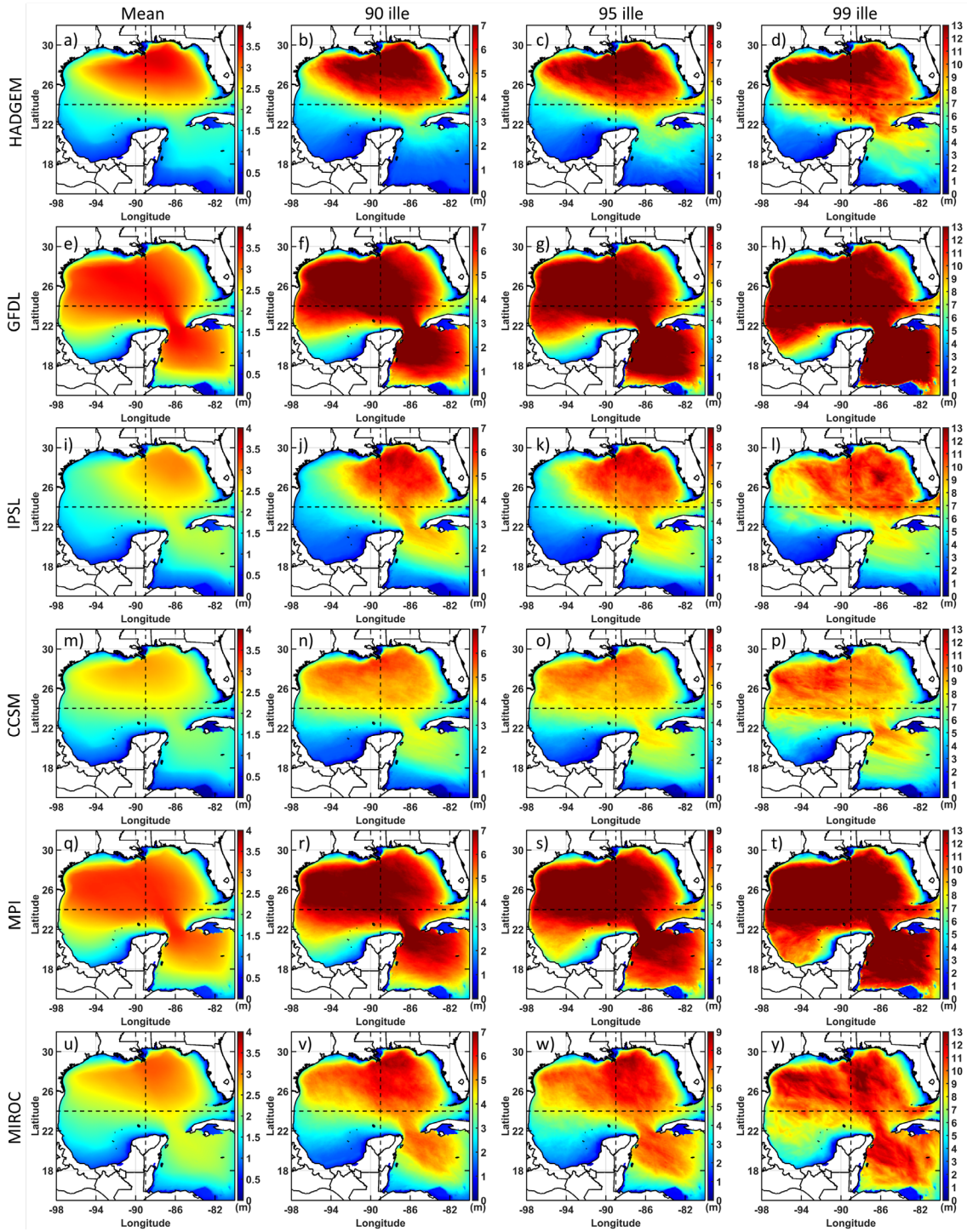


Figure S6. Global circulation models wave conditions for significant wave height in a future climate for HADGEM (a, b, c, d), GFDL (e, f, g, h), IPSL (i, j, k, l), CCSM (m, n, o, p), MPI (q, r, s, t) and MIROC (u, v, x, y) including mean (a, e, i, m, q, u), 90%-ile (b, f, j, n, r, v), 95%-ile (c, g, k, o, s, y) and 99%-ile (d, h, l, p, t, y).

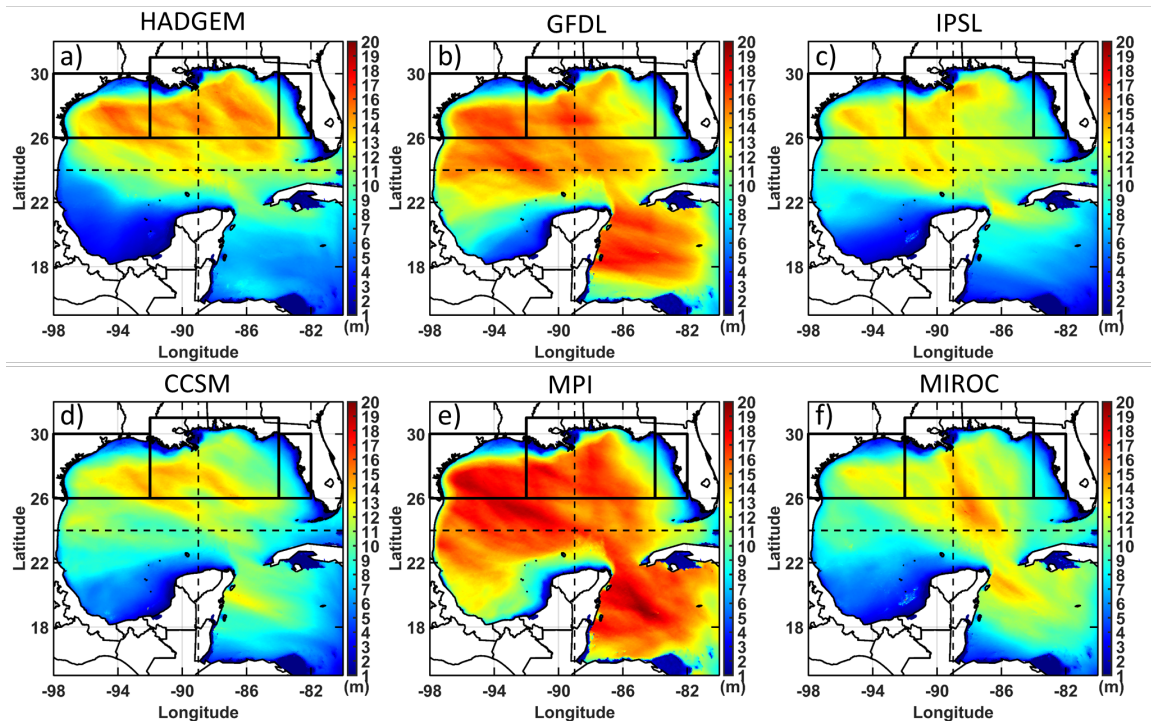


Figure S7. Global circulation model derived events 100-year return period for the present wave climate. a) HADGEM, b) GFDL, c) IPSL, d) CCSM, e) MPI, f) MIROC.

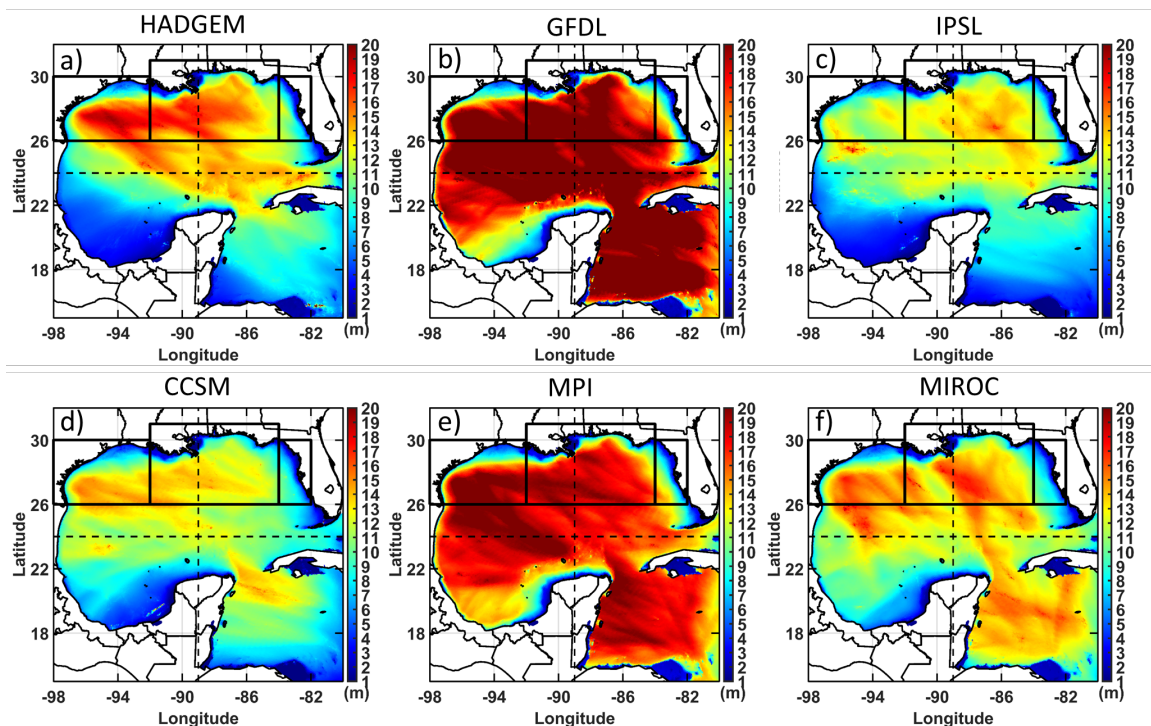


Figure S8. Global circulation model derived events 100-year return period for a future wave climate. a) HADGEM, b) GFDL, c) IPSL, d) CCSM, e) MPI, f) MIROC.

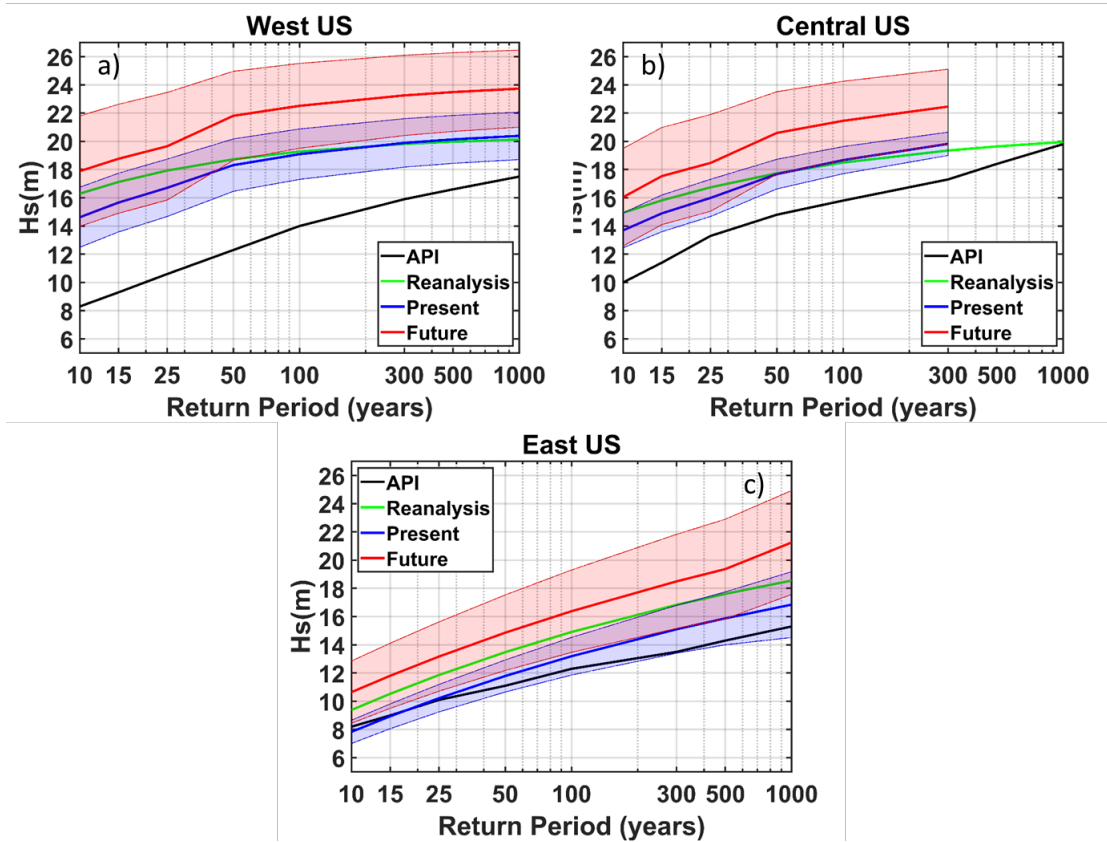


Figure S9. Non corrected values of significant wave height probability in return periods for the different API defined areas in the northern Gulf of Mexico (denoted with the solid black line boxes in a and b of Figure 3), a) West US, b) Central US, and c) East US, showing the return period curves for API and adjusted historic values, and the return periods obtained for reanalysis derived events and for the present and future climates as derived from the GCM derived events ensemble.

Institution	Model name and version	Name used in this article	Reference
National Oceanic and Atmospheric Administration / Geophysical Fluid Dynamics Laboratory (NOAA/GFDL)	Climate Model 3 (CM3)	GFDL	Griffies <i>et al.</i> (2011)
UK Met Office	Hadley Global Environmental Model 2 – Earth System (HADGEM2-ES)	HADGEM	Jones <i>et al.</i> (2011)
Institut Pierre Simon Laplace	CM5A-LR	IPSL	Dufresne <i>et al.</i> (2013)
Center for Climate System Research/National Institute for Environmental Studies/Japan Agency for Marine-Earth Science and Technology	Model for Interdisciplinary Research on Climate 5 (MIROC5)	MIROC	Watanabe <i>et al.</i> (2010)
Max Plank Institute	MPI-ESM-MR	MPI	Giorgetta <i>et al.</i> (2013)
National Center for Atmospheric Research	Community Climate System Model Version 4	CCSM	Gent <i>et al.</i> (2011)

Table S1. Global Circulation Models used to derive present and future climate synthetic tropical cyclones.

Model	Present climate (1975-2005)	Future climate (2070-2100)
NCEP	1566	NA
GFDL	1657	1608
HADGEM	861	609*
IPSL	796	674
MIROC	700	785
MPI	1810	1726
CCSM	1115	1056

* Future climate from 2069 through 2099

Table S2. Number of synthetic events used to characterize the present and future wave climate in the Gulf of Mexico.

		meanm	means	bias	BI	RMS	SI	CC
Hs (m)	42001	2.91	3.32	0.41	0.14	0.88	0.30	1.00
	42002	3.01	3.12	0.11	0.04	0.64	0.21	0.99
	42003	3.23	4.03	0.80	0.25	1.08	0.33	0.99
	42039	3.07	4.23	1.17	0.38	1.71	0.56	0.99
	42040	3.31	4.41	1.10	0.33	1.57	0.48	0.95
	42055	2.21	3.01	0.79	0.36	0.89	0.40	0.99
	42056	3.58	3.92	0.33	0.09	0.64	0.18	0.99
	all	3.07	3.74	0.66	0.22	1.01	0.33	0.99
		meanm	means	bias	BI	RMS	SI	CC
Tp (sec)	42001	8.67	9.14	0.47	0.05	0.72	0.08	0.99
	42002	8.77	8.37	-0.41	-0.05	0.65	0.07	0.99
	42003	8.25	8.91	0.66	0.08	0.86	0.10	0.98
	42039	7.97	9.15	1.18	0.15	1.62	0.20	0.98
	42040	8.05	9.18	1.13	0.14	1.48	0.18	0.95
	42055	7.22	8.24	1.02	0.14	1.07	0.15	0.99
	42056	8.68	8.78	0.11	0.01	0.78	0.09	0.96
	all	8.28	8.85	0.57	0.07	0.84	0.10	0.98
		meanm	means	STDm	STDs	CC	bias	
MWD (deg)	42001	120.12	131.77	0.88	1.03	0.95	-11.65	
	42002	86.69	104.33	0.93	1.14	0.91	-17.64	
	42003	129.96	139.93	1.04	1.19	0.99	-9.97	
	42039	148.67	161.90	0.93	0.82	0.98	-13.23	
	42040	129.78	131.79	0.80	0.69	0.95	-2.01	
	42055	101.09	152.40	1.06	1.16	0.82	-51.31	
	42056	115.18	138.32	0.90	0.90	0.97	-23.15	
	all	119.63	138.37	0.98	1.04	0.99	-18.74	

Table S3. Statistics from model validation using historical events from 1975 through 2020.

References.

- API. (2007). Interim Guidance on Hurricane Conditions in the Gulf of Mexico. *API Recommended Practice, 2INT-MET*, 54.
- API. (2014). Derivation of Metocean Design and Operating Conditions. ANSI/API Recommended practice 2MET. *API Recommended Practice, 2MET*(First Edition), 178.
- Bretschneider, C. L. (1972). A non-dimensional stationary hurricane wave model. *Proceedings of the Annual Offshore Technology Conference, 1972-May*, 151-68. <https://doi.org/10.4043/1517-ms>
- Camargo, S. J. (2013). Global and Regional Aspects of Tropical Cyclone Activity in the CMIP5 Models. *Journal of Climate*, 26(24), 9880–9902. <https://doi.org/10.1175/JCLI-D-12-00549.1>
- Climate, J. O. F., Science, M., Studies, E., Science, M., Science, I., Watanabe, M., et al. (2010). Improved Climate Simulation by MIROC5 : Mean States , Variability , and Climate Sensitivity. *Journal of Climate*, 23(23), 6312–6335. <https://doi.org/10.1175/2010JCLI3679.1>
- Demuth, J. L., DeMaria, M., & Knaff, J. A. (2006). Improvement of Advanced Microwave Sounding Unit Tropical Cyclone Intensity and Size Estimation Algorithms. *Journal of Applied Meteorology and Climatology*, 45(11), 1573–1581. <https://doi.org/10.1175/JAM2429.1>
- Dufresne, J. L., Foujols, M. A., Denvil, S., Caubel, A., Marti, O., Aumont, O., et al. (2013). Climate change projections using the IPSL-CM5 Earth System Model: From CMIP3 to CMIP5. *Climate Dynamics*, 40(9–10), 2123–2165. <https://doi.org/10.1007/s00382-012-1636-1>
- Emanuel, K., & Rotunno, R. (2011). Self-Stratification of Tropical Cyclone Outflow. Part I: Implications for Storm Structure. *Journal of the Atmospheric Sciences*, 68(10), 2236–2249. <https://doi.org/10.1175/JAS-D-10-05024.1>
- Gent, P. R., Danabasoglu, G., Donner, L. J., Holland, M. M., Hunke, E. C., Jayne, S. R., et al. (2011). The community climate system model version 4. *Journal of Climate*, 24(19), 4973–4991. <https://doi.org/10.1175/2011JCLI4083.1>
- Giorgetta, M. A., Jungclaus, J., Reick, C. H., Legutke, S., Bader, J., Böttinger, M., et al. (2013). Climate and carbon cycle changes from 1850 to 2100 in MPI-ESM simulations for the Coupled Model Intercomparison Project phase 5. *Journal of Advances in Modeling Earth Systems*, 5(3), 572–597. <https://doi.org/10.1002/jame.20038>
- Griffies, S. M., Winton, M., Donner, L. J., Horowitz, L. W., Downes, S. M., Farneti, R., et al. (2011). The GFDL CM3 coupled climate model: Characteristics of the ocean and sea ice simulations. *Journal of Climate*, 24(13), 3520–3544. <https://doi.org/10.1175/2011JCLI3964.1>
- Heideman, J. C., & Mitchell, D. A. (2009). Grid Point Pooling in Extreme Value Analysis of Hurricane Hindcast Data. *Journal of Waterway, Port, Coastal, and Ocean Engineering*, 135(2), 31–37. [https://doi.org/10.1061/\(ASCE\)0733-950X\(2009\)135:2\(31\)](https://doi.org/10.1061/(ASCE)0733-950X(2009)135:2(31))
- Jones, C. D., Hughes, J. K., Bellouin, N., Hardiman, S. C., Jones, G. S., Knight, J., et al. (2011). The HadGEM2-ES implementation of CMIP5 centennial simulations. *Geoscientific Model Development*, 4(3), 543–570. <https://doi.org/10.5194/gmd-4->

543-2011

- Landsea, C. W., & Franklin, J. L. (2013). Atlantic Hurricane Database Uncertainty and Presentation of a New Database Format. *Monthly Weather Review*, 141(10), 3576–3592. <https://doi.org/10.1175/MWR-D-12-00254.1>
- Landsea C, W. (2007). Counting Atlantic Tropical Cyclones Back to 1900. *Eos*, 88(18), 197–208. <https://doi.org/10.1029/2007EO180001>
- Lin, N., & Chavas, D. (2012). On hurricane parametric wind and applications in storm surge modeling. *Journal of Geophysical Research*, 117(D9), D09120–D09120. <https://doi.org/10.1029/2011JD017126>
- Oceanweather Inc. (2015). *GOMOS2014: Gulf of Mexico Oceanographic Study 2014. Project Description*. Stamford, CT, USA.
- Powell, M. D., Houston, S. H., Amat, L. R., & Morisseau-Leroy, N. (1998). The HRD real-time hurricane wind analysis system. *Journal of Wind Engineering and Industrial Aerodynamics*, 77–78, 53–64. [https://doi.org/http://dx.doi.org/10.1016/S0167-6105\(98\)00131-7](https://doi.org/http://dx.doi.org/10.1016/S0167-6105(98)00131-7)
- Ruiz-Salcines, P., Salles, P., Robles-Díaz, L., Díaz-Hernández, G., Torres-Freyermuth, A., & Appendini, C. M. (2019). On the use of parametric wind models for wind wave modeling under tropical cyclones. *Water (Switzerland)*, 11(10). <https://doi.org/10.3390/w11102044>